



Reverse Chemical Co-Precipitation: An Effective Method for Synthesis of BiFeO₃ Nanoparticles

H. Sangian*, O. Mirzaee, M. Tajally

Faculty of Materials and Metallurgical Engineering, Semnan University, Semnan, Iran

PAPER INFO

Paper history:

Received 07 March 2017

Accepted in revised form 03 September 2017

Keywords:

Reverse co-precipitation
Bismuth ferrite
Magnetic properties

ABSTRACT

The reverse chemical co-precipitation method was used for synthesis of the pure phase multiferroic BiFeO₃ (BFO) nanoparticles. Influence of different pH values on the microstructure and magnetic properties of the BFO nanopowders was investigated. The phase formation and the existence of impurity phases (like Bi₂₅FeO₃₉ and Bi₂Fe₄O₉) have been studied using X-ray diffractometry (XRD). The morphological features of the nanopowders were characterized using field emission scanning electron microscopy (FESEM) and the presence of absorption bands at 400 to 3600 cm⁻¹ was investigated by Fourier transformed infrared (FTIR) spectroscopy. The magnetic evaluation of the synthesized powders was measured using vibrating sample magnetometry (VSM). The XRD results showed that the BFO powders have R3c crystal structure for all samples and also the diffraction patterns are perfectly indexed to the standard XRD card of BFO. The FESEM micrographs showed irregular shape and average particle size of 71 to 95 and 182 nm for the as-synthesized powders with the pH values of 8.5, 9.5 and 10.5, respectively. The magnetic hysteresis loops indicated antiferromagnetic (weak ferromagnetic) behavior for all samples at room temperature. Whereas the particles size of as-prepared powders were lower than the spiral spin cycloid (62 nm) and because of high surface-to-volume ratio of nanoparticles, which causes more uncompensated spins from the surface, the weak ferromagnetic behavior has been observed.

1. INTRODUCTION

Multiferroic materials simultaneously possess at least two ferroic orders, including (anti)ferromagnetism, ferroelectricity, ferroelasticity and ferrotoroidicity [1]. In the recent decades, multiferroic materials have received much interest because of their novel potential applications in the storage devices [2], actuators [3], microelectronic device [4], non-volatile memories [5] and sensors [6]. Perovskite-type bismuth ferrite (BFO) which emerges interesting physical phenomena such as visible light effect [7], photovoltaic performance [8], giant electrochromic behavior [9], photoluminescence effect [10], magnetoelectric coupling [11] and multiferroic properties [12] has been a suitable candidate for electrooptic [13], catalytic [14], dielectric [15], optical [16] and spintronic [17] applications. Perovskite-type bismuth ferrite (BFO) which possesses high Néel and Curie temperatures ($T_N=370^\circ\text{C}$ and $T_C=825-840^\circ\text{C}$) is the most important single-phase multiferroic which is extensively effective at room

temperatures [18, 19], but owing to some weak properties such as electrical resistivity, leakage current density and low remnant polarization in the bulk form, the BFO industrial application in microelectronic devices has been limited [20-22]. BFO has the perovskite crystallographic structure which belongs to the space group R3c, No.161 with lattice parameters of $a_{rh}=3.965\text{\AA}$ and $\alpha_{rh}=89.3^\circ-89.4^\circ$. Bismuth ferrite has the G-type antiferromagnetic ordering with long period spin cycloid structure (620-640 nm) [20, 23]. The magnetic transition temperature of BFO has been reported previously ($T_N=370^\circ\text{C}$) [24]. Moreover, electrical parameters of BFO such as dielectric constant, polarization hysteresis loops and leakage current, have been studied rather extensively [25-28]. The small band gap of BFO (2.6-2.8 eV) caused its efficient visible light photocatalytic activity [29]. In the early 1967, Achenbach et al. [30] prepared the single phase polycrystalline BFO by solid state reaction of Bi₂O₃ and Fe₂O₃ at temperatures over 700°C. However, because of some disadvantages of their method such as high reaction temperature, large particle size and presence of impurities, new methods such as chemical co-precipitation [31, 32], hydrothermal [33], solvothermal

*Corresponding Author's Email: sangian.hamid@gmail.com (H. Sangian)

[34], sonochemical [35], microemulsion [36], polyacrylamid gel [37], ferrioxalate [38], simple sol-gel [39], combustion synthesis [40], molten salt [41], tartaric acid assisted gel strategy [42], polymeric precursor [43], and mechanochemical procedure [44] are nowadays used for synthesis of BFO nanopowders. Among them, the co-precipitation process involves separation of a solid containing various ions from a solution phase. In this wet chemical process, the acidic cations solution (nitrates or chlorides) and basic precipitant (usually NH_4OH , NaOH and KOH) react together and the amorphous hydroxide precipitates are separated from the solution. The chemical co-precipitation process is divided to four classifications of normal (traditional), reverse (inverse), homogeneous (modified) and fast co-precipitations. The main difference of these processes is the trend of pH changing. In the normal co-precipitation, the precipitating agent is added to the cations solution that causes the pH value rises from acidic region to basic region while in the reverse co-precipitation this addition is inverted thereby the pH value always lies in the basic region. So far, all of the reports have focused on the homogeneous co-precipitation in which the process is very sensitive to pH control [45] which is technologically expensive.

The aim of this paper is to synthesize BFO nanoparticles via reverse chemical co-precipitation method in which there is no need to control the pH and so it is considerably cheaper and easier than homogeneous methods. Reverse co-precipitation has been used effectively for synthesis of some electro-ceramic nanoparticles [46, 47], but to best of our knowledge there is no report on the field of BFO.

2. MATERIALS AND METHODS

The BFO nanoparticles were synthesized by the reverse chemical co-precipitation process. Fig. 1, shows the preparation flowchart which was considered for synthesizing BFO. In this method, bismuth subnitrate $\text{Bi}_5\text{H}_9\text{N}_4\text{O}_{22}$ (Merck kGaA 98.9%) and iron nitrate nonahydrate $\text{Fe}(\text{NO}_3)_3 \cdot 9\text{H}_2\text{O}$ (Merck KGaA 98.9%), (at a molar ratio of 1:1) were dissolved in 2M nitric acid (HNO_3 , scharlau 99.9%) at room temperature. Cation solutions were mixed and stirred severely for 30 minutes to obtain a homogenous transparent mixture. 2M Sodium hydroxide (NaOH) was used as the precipitating agent. In the reverse co-precipitation process, cations solution and precipitating agent were vented into the separator funnel and beaker, respectively. Then cations solution was added dropwise into the precipitating agent under vigorous stirring condition until the pH values of 8.5, 9.5 and 10.5 were reached. The chemical co-precipitation process took about 10 minutes and the suspension was continually washed until the pH of 7 was obtained and the produced

powder was dried in an oven at 80°C for 24h. Finally the dried chunks were crushed in a mortar to obtain the amorphous powders. For crystallization and phase formation, the powders were calcined at 550°C for 1h to obtain pure phase bismuth ferrite.

2.1. Characterization

The calcination temperature was chosen by using thermogravimetric differential thermal analysis (TG-DTA) with heating rate of $5^\circ\text{C}/\text{min}$. In order to identify purity of calcined parent phases and their presence in composite specimens, an X-ray diffractometer (BRUKER X-Ray) using the $\text{Cu-K}\alpha$ radiation and scan rate of $0.05^\circ/\text{min}$ in the scattering angular range (2θ) of 10 - 90° was utilized. Fourier transformed infrared (FT-IR) spectrum was recorded using a spectrometer (FT-IR SHIMADZU). The morphology and size distribution of the BFO powders were obtained by using the field emission scanning electron microscope (MIRA3- TSCAN). The magnetic hysteresis loops with external magnetic field of ± 1.0 T were measured at room temperature using a vibration sample magnetometer (VSM AGFM).

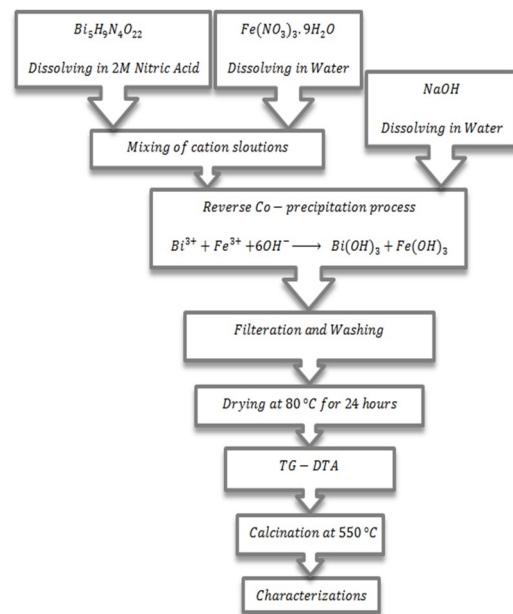


Figure 1. Preparation flowchart of the reverse co-precipitation procedure for synthesis of the BFO.

3. RESULT AND DISCUSSION

3.1. Thermal behavior

The TG-DTA curves of the un-calcined powders synthesized by the reverse co-precipitation method with the pH value of 9.5 are shown in Fig. 2. The peak located at 263.2°C in the DTA curve is related to the decomposition of hydrates, nitrates and retained water on the surface of nanoparticles, which is accompanied by a large weight loss in this stage. The peak presented at 470.8°C , corresponds to crystallization of BFO powders, which

was used for selecting the appropriate calcination temperature of 550°C in this study. Formation of the BFO is based on the following chemical reaction [45]. After decomposition of the compounds and formation of the crystallized phase, the TG curve shows the total weight loss of approximately 16% equal to the calculated weight loss for the total calcination reaction, which is related to releasing H₂O during the crystallization reaction.



Usually, a ferroelectric to paraelectric phase transition can be seen in the BFO by the low intensity peak in the DTA without any weight loss in the TG curves [48]. This situation in the TG-DTA curve is presented at 818.7°C [49].

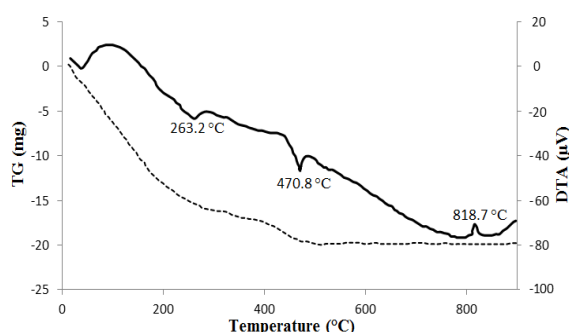


Figure 2. TG-DTA curves of the precursor sample synthesized with pH value of 9.5.

3.2. XRD analysis

The phase formation of the BFO samples which were calcined at 550°C was characterized using X-ray diffraction (XRD). Fig. 3. demonstrates the XRD patterns of reversely co-precipitated samples with pH values of 8.5, 9.5 and 10.5. Whereas the distribution of Bi and Fe ions was homogeneous in the reverse co-precipitation, and all samples show pure phase BFO.

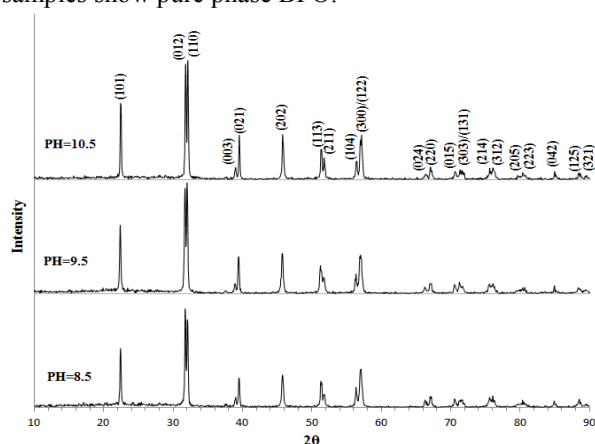


Figure 3. XRD patterns of the calcined BFO samples with different pH values.

However, diffraction patterns of calcined samples match perfectly with the standard card of JCPDS No. 00-014-0181, confirming that they contain pure BiFeO₃ without any unwanted secondary phase. Bravias lattice was primitive cubic ($a=3.95\text{\AA}$, space group R3c No.161). The maximum crystallite size (54 nm) was calculated for pH = 10.5.

3.3. FT-IR spectroscopy

The FT-IR spectra of the precursor and crystalline BFO powders derived from the reverse co-precipitation are shown in Fig. 4. Which were calcined at 550°C. The spectra are in good agreement with the TG-DTA curve. After calcinations, some of the bands are eliminated or moved up, which can be related to compounds evaporation or their contribution in the reaction [50]. The peaks at 3417 cm⁻¹ and 1625 cm⁻¹ are attributed to the stretching and bending of the H₂O molecules, respectively [51]. In the precursor sample, the strong peaks near 1384 cm⁻¹ and 846 cm⁻¹ can be related to the variation of NO₃⁻ [52, 53]. The ferrite characteristic bands in the range of 400-600 cm⁻¹ are associated with metallic ions. The band with a higher wave number (around 575 cm⁻¹) is connected with the intrinsic characteristic stretching vibration of metal at tetrahedral sites and the other one with lower intensity and wavenumber (around 408 cm⁻¹) is related to the intrinsic characteristic stretching vibration of metal at octahedral sites [54]. These peaks are characteristic for BFO with perovskite structure.

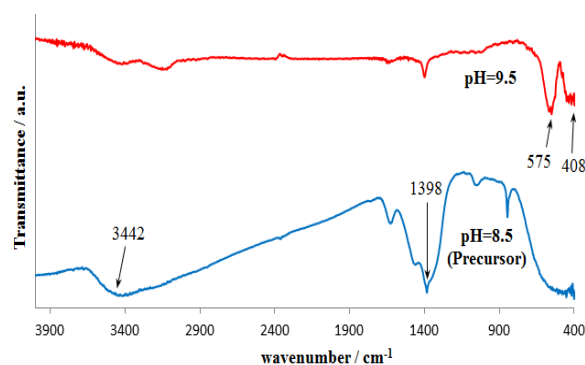


Figure 4. FT-IR spectrum of the BFO powders precursor and calcined samples.

3.4. Microstructural observation

The morphological features of powder samples, particle size and distribution were observed using a field emission scanning electron microscopy (FESEM), equipped with energy dispersive X-ray spectrometer (EDX). Fig. 5 depicts the FESEM micrographs of the precursor powder with ultrafine grains (less than 10 nm) prepared by the reverse chemical co-precipitation. The agglomeration of the particles is clearly seen. The reason for agglomeration is fast (uncontrolled) precipitation reaction and also the tendency to minimize the surface free energy of nanoparticles and the strong

attractive interaction between BFO nanoparticles. The EDX analysis of the reversely synthesized sample with the pH value of 9.5 is illustrated in Fig. 6. This pattern confirms that the elements in the samples are limited to Bi, O and Fe. The atomic percent of Bi, Fe and O are listed in the inset table in Fig. 6. The Bi/Fe ratio is 1.053, which is very close to the stoichiometric ratio for pure phase of BFO. Fig. 7 shows the FESEM micrographs of BFO samples of the reversely co-precipitated powders with different pH values calcined at 550 °C for 1h. Agglomerated morphology in Fig. 7 and granular shape of particles in all samples can clearly be seen. The micrographs showed the average particle sizes of 71 to 95 and 182 nm for the as-synthesized powders with the pH values of 8.5, 9.5 and 10.5, respectively. To Considering the Fig. 7, the average size of particles increases with increasing the pH value. Concentration of OH⁻ ions increases with increasing the pH value in the solution and results in accelerated precipitation reaction that causes the larger agglomerated precipitates and particle size. Therefore, final particle size increases with increasing the pH value as shown in the micrographs.

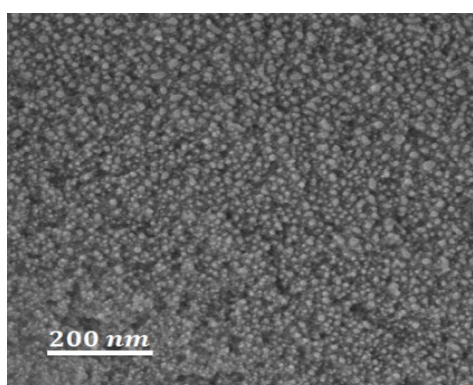


Figure 5. FESEM micrographs of synthesized precursor with the pH value of 9.5.

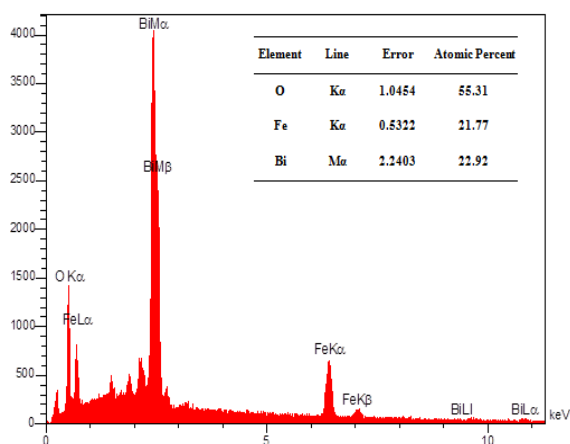


Figure 6. EDX analysis of the reversely synthesized sample with the pH value of 9.5.

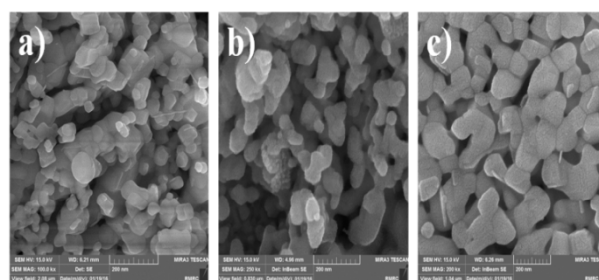


Figure 7. FESEM micrographs of the calcined BFO samples synthesized by the reverse co-precipitation method with the pH= 8.5, 9.5 and 10.5.

3.5. Magnetization

The magnetic hysteresis loops of the calcined BFO nanoparticles synthesized by the reverse co-precipitation with an applied magnetic field in the range of ± 1.0 T at room temperature was also measured in this paper. As shown in Fig. 8, the magnetic hysteresis loops showed antiferromagnetic behavior and the magnetization is increased with decrement of the pH value. The important factor for the appearance of magnetization in antiferromagnetic materials is the particles size effect and specific surface area of particles[55]. Due to higher surface-to-volume ratio in produced nanoparticles, the uncompensated surface spins do not depend magnetically on spin arrangement. Also, the emersion of magnetization in nano-sized BFO can be explained as follows:

The uncompensated spins from the surface can improve the magnetization of BFO nanoparticle [56]. In the achieved BFO powders, the particle size decreases as the pH value decreases. Thus, the large fraction of uncompensated spins from the surface causes enhancement of magnetic properties due to high surface-to-volume ratio in the nanoparticles [57].

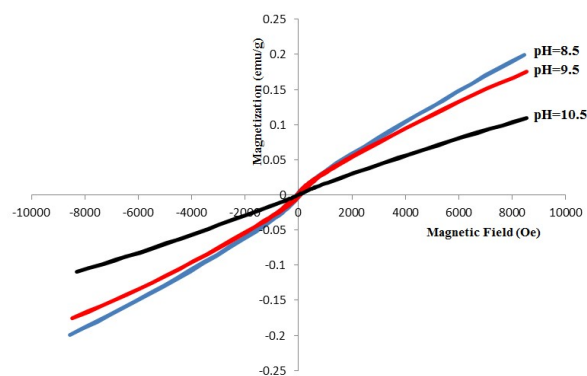


Figure 8. The magnetization curves of the as-prepared powders with different pH values.

4. CONCLUSIONS

The BFO nanoparticles were successfully synthesized via the reverse chemical co-precipitation method. The TG-DTA analysis revealed that the crystallization of

BFO powders occurs at 470.8 °C, and the peak at 818.7 °C in the heating cycle obtains the Curie point. The XRD patterns indicate the formation of pure phase in this method. The electron microscopy of the samples showed that the particle size increases as the pH value increases. The magnetic hysteresis loops confirmed an antiferromagnetic (weak ferromagnetic) behavior of the BFO nanoparticles synthesized by reverse co-precipitation at room temperature. The average diameters of the achieved BFO powders are smaller than the spiral spin structure period. Besides, as the pH value decreases, the particle size decreases that is responsible for the large fraction of uncompensated spins from the surface, which causes improvement of magnetization due to the high surface-to-volume ratio of the nanoparticles.

5. ACKNOWLEDGMENTS

The authors would like to thank laboratory department of materials and metallurgical engineering, Semnan University.

REFERENCES

- Eerenstein, W., Mathur, N. and Scott, J.F., "Multiferroic and magnetoelectric materials", *Nature*, Vol. 442, (2006), 759-765.
- Scott, J., "Data storage: Multiferroic memories", *Nature Materials*, Vol. 6, (2007), 256-257.
- Shami, M.Y., Awan, M. and Anis-ur-Rehman, M., "Effect of pH Variation on Structural and Dielectric Properties of Co-precipitated Nanostructured Multiferroic BiFeO₃", *Journal of Superconductivity and Novel Magnetism*, Vol. 26, (2013), 1071-1074.
- Markiewicz, E., Szot, K., Hilczer, B. and Pietraszko, A.A., "BiFeO₃ single crystal as resistive switching element for application in microelectronic devices", *Phase Transitions*, Vol. 86, (2013), 284-289.
- Guo, R., You, L., Zhou, Y., Lim, Z.S., Zou, X., Chen, L., Ramesh, R. and Wang, J., "Non-volatile memory based on the ferroelectric photovoltaic effect", *Nature Communications*, Vol. 4, (2013).
- Das, S., Rana, S., Mursalin, S.M., Rana, P. and Sen, A., "Sonochemically prepared nanosized BiFeO₃ as novel SO₂ sensor", *Sensors and Actuators B: Chemical*, Vol. 218, (2015), 122-127.
- Gao, T., Chen, Z., Zhu, Y., Niu, F., Huang, Q., Qin, L., Sun, X. and Huang, Y., "Synthesis of BiFeO₃ nanoparticles for the visible-light induced photocatalytic property", *Materials Research Bulletin*, Vol. 59, (2014), 6-12.
- Hung, C.-M., Tu, C.-S., Yen, W., Jou, L., Jiang, M.-D. and Schmidt, V., "Photovoltaic phenomena in BiFeO₃ multiferroic ceramics", *Journal of Applied Physics*, Vol. 111, (2012), 07D912.
- Sando, D., Yang, Y., Bousquet, E., Carrétero, C., Garcia, V., Fusil, S., Dolfi, D., Barthélémy, A., Ghosez, P. and Bellaiche, L., "Large elasto-optic effect and reversible electrochromism in multiferroic BiFeO₃", *Nature Communications*, Vol. 7, (2016).
- Prashanthi, K., Thakur, G., Thundat, T., "Surface enhanced strong visible photoluminescence from one-dimensional multiferroic BiFeO₃ nanostructures", *Surface Science*, Vol. 606, (2012), 83-86.
- Ederer, C. and Spaldin, N.A., "Weak ferromagnetism and magnetoelectric coupling in bismuth ferrite", *Physical Review B*, Vol. 71, (2005), 060401.
- Kim, A., Han, S.-H., Kim, J.-S. and Cheon, C.-I., "Multiferroic Property and Crystal Structural Transition of BiFeO₃-SrTiO₃ Ceramics", *Journal of the Korean Ceramic Society*, Vol. 48, (2011), 307-311.
- Sando, D., Hermet, P., Allibe, J., Bourderionnet, J., Fusil, S., Carrétero, C., Jacquet, E., Mage, J.-C., Dolfi, D. and Barthélémy, A., "Linear electro-optic effect in multiferroic BiFeO₃ thin films", *Physical Review B*, Vol. 89, (2014), 195106.
- Zou, J., Gong, W., Ma, J., Li, L. and Jiang, J., "Efficient Catalytic Activity BiFeO₃ Nanoparticles Prepared by Novel Microwave-Assisted Synthesis", *Journal of Nanoscience and Nanotechnology*, Vol. 15, (2015), 1304-1311.
- Liu, Z., Liang, S., Li, S., Zhu, Y., Zhu, X., "Synthesis, microstructural characterization, and dielectric properties of BiFeO₃ microcrystals derived from molten salt method", *Ceramics International*, Vol. 41, (2015), 19-25.
- Shima, H., Naganuma, H., Iijima, T., Nakajima, T. and Okamura, S., "The Optical Property of Multiferroic BiFeO₃ Films", *Integrated Ferroelectrics*, Vol. 106, (2009), 11-16.
- Marrows, C., Chapon, L. and Langridge, S., "Spintronics and functional materials", *Materials Today*, Vol. 12, (2009), 70-77.
- Bhide, V.G. and Multani, M.S., "Mössbauer effect in ferroelectric-antiferromagnetic BiFeO₃", *Solid State Communications*, Vol. 3, (1965), 271-274.
- Michel, C., Moreau, J.-M., Achenbach, G.D., Gerson, R. and James, W.J., "The atomic structure of BiFeO₃", *Solid State Communications*, Vol. 7, (1969), 701-704.
- Park, T.-J., Papaefthymiou, G.C., Viescas, A.J., Moodenbaugh, A.R. and Wong, S.S., "Size-dependent magnetic properties of single-crystalline multiferroic BiFeO₃ nanoparticles", *Nano Letters*, Vol. 7, (2007), 766-772.
- Yang, H., Wang, Y.Q., Wang, H. and Jia, Q.X., "Oxygen concentration and its effect on the leakage current in BiFeO₃ thin films", *Applied Physics Letters*, Vol. 96, (2010), 012909.
- Uniyal, P. and Yadav, K.L., "Observation of the room temperature magnetoelectric effect in Dy doped BiFeO₃", *Journal of Physics: Condensed Matter*, Vol. 21, (2009), 012205.
- Safi, R. and Shokrollahi, H., "Physics, chemistry and synthesis methods of nanostructured bismuth ferrite (BiFeO₃) as a ferroelectro-magnetic material", *Progress in Solid State Chemistry*, Vol. 40, (2012), 6-15.
- Blaauw, C. and Van der Woude, F., "Magnetic and structural properties of BiFeO₃", *Journal of Physics C: Solid State Physics*, Vol. 6, (1973), 1422.
- Jia, D.-C., Xu, J.-H., Ke, H., Wang, W. and Zhou, Y., "Structure and multiferroic properties of BiFeO₃ powders", *Journal of the European Ceramic Society*, Vol. 29, (2009), 3099-3103.
- Pradhan, S.K. and Roul, B.K., "Improvement of multiferroic and leakage property in monophasic BiFeO₃", *Physica B: Condensed Matter*, Vol. 406, (2011), 3313-3317.
- Shami, M.Y., Awan, M.S. and Anis-ur-Rehman, M., "Phase pure synthesis of BiFeO₃ nanopowders using diverse precursor via co-precipitation method", *Journal of Alloys and Compounds*, Vol. 509, (2011), 10139-10144.
- Shokrollahi, H., "Magnetic, electrical and structural characterization of BiFeO₃ nanoparticles synthesized by co-precipitation", *Powder Technology*, Vol. 235, (2013), 953-958.
- Gao, F., Chen, X., Yin, K., Dong, S., Ren, Z., Yuan, F., Yu, T., Zou, Z. and Liu, J.M., "Visible-Light Photocatalytic Properties

- of Weak Magnetic BiFeO₃ Nanoparticles", *Advanced Materials*, Vol. 19, (2007), 2889-2892.
30. Achenbach, G., James, W. and Gerson, R., "Preparation of Single-Phase Polycrystalline BiFeO₃", *Journal of the American Ceramic Society*, Vol. 50, (1967), 437-437.
 31. Muneeswaran, M., Jegatheesan, P. and Giridharan, N., "Synthesis of nanosized BiFeO₃ powders by co-precipitation method", *Journal of Experimental Nanoscience*, Vol. 8, (2013), 341-346.
 32. Xie, H., Wang, K., Jiang, Y., Zhao, Y. and Wang, X. "An Improved Co-precipitation Method to Synthesize Three Bismuth Ferrites, Synthesis and Reactivity in Inorganic", *Metal-Organic, and Nano-Metal Chemistry*, Vol. 44, (2014), 1363-1367.
 33. Liu, B., Hu, B. and Du, Z., "Hydrothermal synthesis and magnetic properties of single-crystalline BiFeO₃ nanowires", *Chemical Communications*, Vol. 47, (2011), 8166-8168.
 34. Das, S. and Basu, S., Solvothermal synthesis of nano-to-submicrometer sized BiFeO₃ and Bi-Fe-oxides with various morphologies", *Journal of nanoscience and nanotechnology*, Vol. 9, (2009), 5622-5626.
 35. Fang, L., Liu, J., Ju, S., Zheng, F., Dong, W. and Shen, M., "Experimental and theoretical evidence of enhanced ferromagnetism in sonochemical synthesized BiFeO₃ nanoparticles", *Applied Physics Letters*, Vol. 97, (2010), 242501.
 36. Das, N., Majumdar, R., Sen, A., Maiti, H.S., "Nanosized bismuth ferrite powder prepared through sonochemical and microemulsion techniques", *Materials Letters*, Vol. 61, (2007), 2100-2104.
 37. Xian, T., Yang, H., Shen, X., Jiang, J.L., Wei, Z.Q. and Feng, W.J., "Preparation of high-quality BiFeO₃ nanopowders via a polyacrylamide gel route", *Journal of Alloys and Compounds*, Vol. 480, (2009), 889-892.
 38. Ghosh, S., Dasgupta, S., Sen, A. and Maiti, H.S., "Low temperature synthesis of bismuth ferrite nanoparticles by a ferrioxalate precursor method", *Materials Research Bulletin*, Vol. 40, (2005), 2073-2079.
 39. Dhir, G., Uniyal, P. and Verma, N.K., "Sol-gel synthesized BiFeO₃ nanoparticles: Enhanced magnetoelectric coupling with reduced particle size", *Journal of Magnetism and Magnetic Materials*, Vol. 394, (2015), 372-378.
 40. Yang, J., Li, X., Zhou, J., Tang, Y., Zhang, Y. and Li, Y., "Factors controlling pure-phase magnetic BiFeO₃ powders synthesized by solution combustion synthesis", *Journal of Alloys and Compounds*, Vol. 509, (2011), 9271-9277.
 41. Zheng, X., Chen, P., Ma, N., Ma, Z. and Tang, D., "Synthesis and dielectric properties of BiFeO₃ derived from molten salt method", *Journal of Materials Science: Materials in Electronics*, Vol. 2, (2012), 990-994.
 42. Wang, X., Zhang, Y.g. and Wu, Z., "Magnetic and optical properties of multiferroic bismuth ferrite nanoparticles by tartaric acid-assisted sol-gel strategy", *Materials Letters*, Vol. 64, (2010), 486-488.
 43. Popa, M., Crespo, D., Calderon-Moreno, J.M., Preda, S. and Fruth, V., "Synthesis and structural characterization of single-phase BiFeO₃ powders from a polymeric precursor", *Journal of the American Ceramic Society*, Vol. 90, (2007), 2723-2727.
 44. Szafraniak, I., Połomska, M., Hilczer, B., Pietraszko, A. and Kępiński, L., "Characterization of BiFeO₃ nanopowder obtained by mechanochemical synthesis", *Journal of the European Ceramic Society*, Vol. 27, (2007), 4399-4402.
 45. Ke, H., Wang, W., Wang, Y., Xu, J., Jia, D., Lu, Z. and Zhou, Y., "Factors controlling pure-phase multiferroic BiFeO₃ powders synthesized by chemical co-precipitation", *Journal of Alloys and Compounds*, Vol. 509, (2011), 2192-2197.
 46. Marlot, C., Barraud, E., Le Gallet, S., Eichhorn, M. and Bernard, F., "Synthesis of YAG nanopowder by the co-precipitation method: Influence of pH and study of the reaction mechanisms", *Journal of Solid State Chemistry*, Vol. 191, (2012), 114-120.
 47. Huixia, F., Baiyi, C., Deyi, Z., Jianqiang, Z. and Lin, T., "Preparation and characterization of the cobalt ferrite nanoparticles by reverse coprecipitation", *Journal of Magnetism and Magnetic Materials*, Vol. 356, (2014), 68-72.
 48. Das, S., Choudhary, R., Bhattacharya, P., Katiyar, R., Dutta, P., Manivannan, A. and Seehra, M., "Structural and multiferroic properties of La-modified BiFeO₃ ceramics", *Journal of applied physics*, Vol. 101, (2007), 034104.
 49. Basiri, M., Shokrollahi, H. and Isapour, G., "Effects of La content on the magnetic, electric and structural properties of BiFeO₃", *Journal of Magnetism and Magnetic Materials*, Vol. 354, (2014), 184-189.
 50. Liu, Y., Zhang, Y., Feng, J., Li, C., Shi, J. and Xiong, R., "Dependence of magnetic properties on crystallite size of CoFe₂O₄ nanoparticles synthesised by auto-combustion method", *Journal of Experimental Nanoscience*, Vol. 4, (2009), 159-168.
 51. Wang, J., Wei, Y., Zhang, J., Ji, L., Huang, Y., Chen, Z., "Synthesis of pure-phase BiFeO₃ nanopowder by nitric acid-assisted gel", *Materials Letters*, Vol. 124, (2014), 242-244.
 52. Biasotto, G., Simões, A.Z., Foschini, C.R., Antônio, S.G., Zaghet, M.A. and Varela, J.A., "A novel synthesis of perovskite bismuth ferrite nanoparticles", *Processing and Application of Ceramics*, Vol. 5, (2011), 171-179.
 53. Ilić, N.I., Džunuzović, A.S., Bobić, J.D., Stojadinović, B.S., Hammer, P., Vijatović Petrović, M.M., Dohčević-Mitrović, Z.D. and Stojanović, B.D., "Structure and properties of chemically synthesized BiFeO₃. Influence of fuel and complexing agent", *Ceramics International*, Vol. 41, (2015), 69-77.
 54. Mohamed, R., Rashad, M., Haraz, F. and Sigmund, W., "Structure and magnetic properties of nanocrystalline cobalt ferrite powders synthesized using organic acid precursor method", *Journal of Magnetism and Magnetic Materials*, Vol. 322, (2010), 2058-2064.
 55. Mohammadi, S., Shokrollahi, H. and Basiri, M., "Effects of Gd on the magnetic, electric and structural properties of BiFeO₃ nanostructures synthesized by co-precipitation followed by microwave sintering", *Journal of Magnetism and Magnetic Materials*, Vol. 375, (2015), 38-42.
 56. Wang, J., Neaton, J., Zheng, H., Nagarajan, V., Ogale, S., Liu, B., Viehland, D., Vaithyanathan, V., Schlom, D. and Waghmare, U., "Epitaxial BiFeO₃ multiferroic thin film heterostructures", *Science*, Vol. 299, (2003), 1719-1722.
 57. Mohammadi, S., Shokrollahi, H. and Basiri, M.H., "Effects of Gd on the magnetic, electric and structural properties of BiFeO₃ nanostructures synthesized by co-precipitation followed by microwave sintering", *Journal of Magnetism and Magnetic Materials*, Vol. 375, (2015), 38-42.